Supporting Information for

Bridging Oxygen Atoms in Trigonal Prism Units Driven Strong Second-Harmonic-Generation Efficiency in Sr$_3$Ge$_2$O$_4$Te$_3$

Mengran Sun,[a,b,c] Wenhao Xing,[d] Ming-Hsien Lee,[e,*] and Jiyong Yao[a,b,*]

a Beijing Center for Crystal Research and Development, Key Lab of Functional Crystals and Laser Technology,

Technical Institute of Physics and Chemistry, Chinese Academy of Sciences, Beijing 100190, P. R. China.

b Center of Materials Science and Optoelectronics Engineering, University of Chinese Academy of Sciences,

Beijing 100049, P. R. China.

c University of Chinese Academy of Sciences, Beijing 100049, P. R. China.

d Institute of Chemical Materials, China Academy of Engineering Physics, Mianyang 621900, P. R. China.

e Department of Physics, Tamkang University, Tamsui, New Tapei 25137, Taiwan.

*Corresponding author:

Ming-Hsien Lee; mhslee@mail.tku.edu.tw.

Jiyong Yao; jyao@mail.ipc.ac.cn.

<center>**Experimental details**</center>

Caution! Toxic HgTe was used; safeguards should be taken.

Reagent. All staring materials, Sr (99.99%), GeO_2 (99.99%), Ge (99.99%), HgTe (99%), and Te (99.999%) were directly purchased from Aladdin Co., Ltd. without further purification. The synthesis of binary materials SrTe and GeTe are to heat the stoichiometric mixture of the elements in vacuum flame-sealed silica tubes. All manipulations are carried out in an Ar-filled glove box.

1. **Single Crystal Growth**

The $Sr_3Ge_2O_4Te_3$ single crystals were grown via spontaneously crystallization. SrTe (0.93 mmol, 0.2g), HgTe (0.31 mmol, 0.1g), GeTe (0.31 mmol, 0.062g), and GeO_2 (0.31 mmol, 0.032g) were thoroughly ground and loaded into a quartz tube. The HgTe was used as flux. The tube containing the raw materials was sealed under a 10^{-3} pa vacuum and placed in a tube furnace. Then, set the heating program as follows: the tube was heated from room temperature to 1173 K in 17 h, kept for 50 h, then slowly cooled to 773 K at a rate of 3 K/h, and finally cooled to room temperature within 5h. The yellow-brown block-like crystals of $Sr_3Ge_2O_4Te_3$ can be obtained with a yield of 70% (base on Ge). These crystals are not sensitive to oxygen and water in the air.

2. **Structure Determination**

A $Sr_3Ge_2O_4Te_3$ crystal without cracks was selected for single-crystal X-ray diffraction on a Rigaku AFC10 diffractometer equipped with a graphite-monochromated Mo-K_α (λ = 0.71073 Å) radiation at 297(2) K. CrysAlispro software

was used for data reduction, and Multi-scan method was used for absorption correction. Structure solution and refinement of $Sr_3Ge_2O_4Te_3$ were carried out with the direct method and full-matrix least squares on F^2 with SHELXL-2014 package.[1] The crystallographic data and structure refinement details of $Sr_3Ge_2O_4Te_3$ are exhibited in Table S1. The atomic coordinates, equivalent isotropic displacement parameters, and bond-valence sum (BVS) are listed in Table S2. The selected bond lengths and angles are summarized in Table S3.

3. Polycrystalline Synthesis

The polycrystalline powder of $Sr_3Ge_2O_4Te_3$ adopts the traditional high-temperature solid-state synthesis method by heating the stoichiometric mixture of the elements. The mixture of 0.378 g SrTe and 0.122 g GeO_2 was evenly ground and placed into a quartz tube, which was sealed under high vacuum of 10^{-3} Pa. This sample were gradually heated to 973 K in 10 h, maintained for 50 h, and finally cooled to room temperature (RT).

4. Properties Characterization

Powder X-ray Diffraction

A Bruker D8 Focus diffractometer equipped with Cu-K_α ($\lambda = 1.5418$ Å) radiation was used to perform the powder X-ray diffraction of $Sr_3Ge_2O_4Te_3$. The diffraction pattern from 10° to 70° was collected with the parameters of a scanning step width of 0.02° and a counting time of 0.1 s/step.

Element Analysis

The FEI Quanta 650FEG scanning electron microscope (SEM) equipped with energy−dispersive X−ray (EDX) was used to perform the elemental analysis on the single crystal of $Sr_3Ge_2O_4Te_3$.

Optical Characterizations

A Carry 5000 UV-vis-NIR spectrophotometer with a diffuse reflectance accessory was applied to obtain the diffuse-reflectance spectra of $Sr_3Ge_2O_4Te_3$ and polytetrafluoroethylene (as a reference) in the range of $2500 - 200$ nm. A Lab RAM Aramis spectrometer equipped with a 532 nm laser was used to collect the Raman spectrum of $Sr_3Ge_2O_4Te_3$ in the range of 100 to 1000 cm^{-1} at RT. A Excalibur 3100 Fourier Transform Infrared Spectrometer was used to collect the IR spectrum in the range of 400-4000 cm^{-1}. The samples for IR measurement were prepared by fully grinding $Sr_3Ge_2O_4Te_3$ crystals with KBr powder (1:100 mass ratio).

Thermal Properties

A Labsys TG-DTA16 (SETARAM) thermal analyzer was used to evaluate the thermal stability of $Sr_3Ge_2O_4Te_3$. Appropriate amount of $Sr_3Ge_2O_4Te_3$ polycrystalline powder was placed into a quartz tube with the size of 5 mm (o.d.) × 3 mm (i.d.) and eventually sealed the tube at 10^{-6} Pa. During the measurement process, the nitrogen flow was circulated at a flow rate of about 15 mL/ min, and the temperature of the tube was heated from RT to 1273 K at a rate of 15 K / min, and then gradually lowered to RT at the same rate.

Powder SHG Measurement

The SHG intensity of $Sr_3Ge_2O_4Te_3$ was estimated by Kurtz-Perry technique with a

2090 nm laser generated by a Q-switch Ho:Tm:Cr:YAG laser.[2] The polycrystalline sample of $Sr_3Ge_2O_4Te_3$ was sieved into five particle ranges, namely 20-50, 50-90, 90-125, 125-150, and 150-200 μm, and then these samples of different particle sizes were load into custom holders with a thickness of 1mm. In addition, the single crystals of the traditional material AGSe were fully ground and sieved into the same particle size ranges as mentioned above for reference.

Laser Damage Threshold Measurement

The powder LDT values of $Sr_3Ge_2O_4Te_3$ and the benchmark material AGSe were evaluated by the single-pulse method. Glass cover slips were used to place the samples of the same particle size range (40-90 μm), and then fixed with rubber pads in a 1 mm thick aluminum holder. The molds were placed in the experimental light path, and the holders were irradiated by a 1064 nm laser with an τ_p = 8 ns pulse width. Then, the surface of these two samples were observed under an optical microscope with increasing laser power until the dazzling light spot emitted by the sample surface due to damage was appeared. Finally, the laser power and the area of the damage point were recorded to calculate the LDT values of these two samples.

5. Theoretical Calculations

In this study, a DFT code CASTEP were used.[3-5] From Materials Studio CASTEP Pseudopotential Library, qc-tuning type Optimized Norm-conserving pseudopotential were selected and used at Kinetic Energy cutoff 750 eV, which corresponds to within 0.1 eV per atom convergence of total energy.[6-7] Uniform Monkhorst-Pack k-point sampling (symmetrized) for SCF has 0.08 Angs.$^{-1}$ Sampling point Separation, for BS /

Optics calculation 0.04 Angs.[-1]. And the total valence electrons are distributed as Sr $4s^24p^65s^2$, Ge $4s^24p^2$, Te $5s^25p^4$, and O $2s^22p^4$ electrons. Convergence test of such sampling has been performed to ensure reasonable convergence of resulting optical properties. To calculate birefringence and SHG, both methods available to CASTEP were used, one based on a sum-over-states[8-9] type formalism referred as optical properties calculation, another based on E-field DFPT[10-11] perturbation recently implemented within CASTEP.
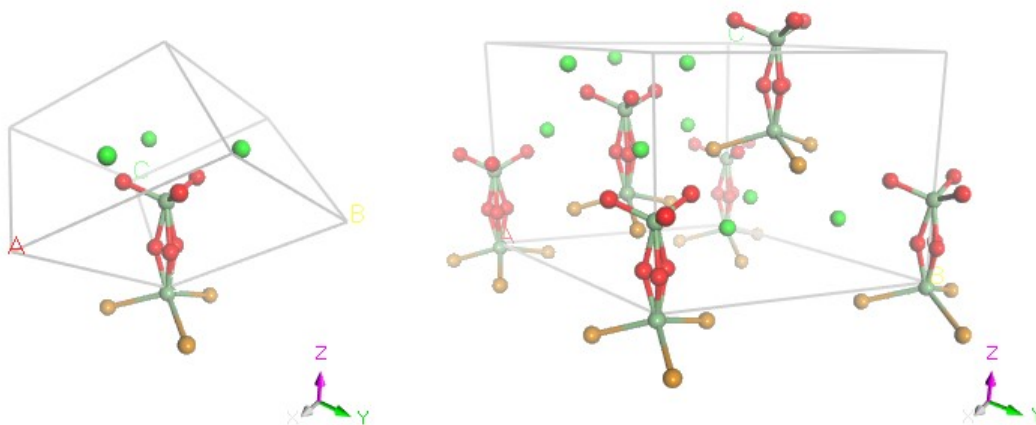
The experimentally determined crystal structure has non-unity SOF (site occupation fraction) for the bridge oxygens, as indicated in Figure S1. This presents a challenge to first principles calculation. Supercell or VCA (Vertural Crystal Approximation) were two common ways to detail with such statistical randomness of ions in a real crystal. Here we took a different approach, namely model the crystal with and ideal structure. This has the advantage of yielding simple and clear results for analysis and interpretation, and also save computational time significantly. Observation of Figure S1 suggests that the small deviation is likely due to spontaneous symmetry breaking of [$Ge_2Te_3O_4$] units having non-180 degrees Ge−O−Ge bond angle, but only a small deviation from 180 degrees.

With an idealized structure indicated in Figure S2, here we replace these oxygens with a whole oxygen at their averaged position, this action does not change the symmetry. Three 1/3 SOF oxygen is located very near, with the averaged position of the new whole oxygen site is only 0.443 Angs. Away. As the change is a shift perpendicular to the O−Ge and O−Te bonds, the two bond lengths of Ge−O−Ge is

barely changed, only bond angle become 180 degrees.

Optical property calculations were carried out for determined (idealized) crystal structure and fully (cell-volume and ion positions) relaxed one, and the results are given in Tables S4 and S5, respectively. Among them, Table S4 shows results from both E-field DFPT calculations and sum-over-states optical properties calculations, the results on birefringence is consistence between these two methods. The d_{ij} obtained by the two methods are not consistent, but the ones calculated by the E-field method are more credible (after all, sum-over-states method is zero-order perturbation, and DFPT is linear response, that is, first-order perturbation). Also we noticed relaxed structure has slightly smaller d_{ij} and birefringence, but still remain consistent between results, see Table S5. Besides, these results show that scissors correction slightly decreases Δn and d_{ij} (an expected effect from SOS formulism, bang-gap value appears in the denominator), whereas ion and cell relaxation slightly increases n and d_{ij}.

6. Figure S1

Experimentally determined strcture in rhombohedral (left) and hexagonal (right) unit cells. Each triple oxygen ions has 1/3 fractional occupiency.
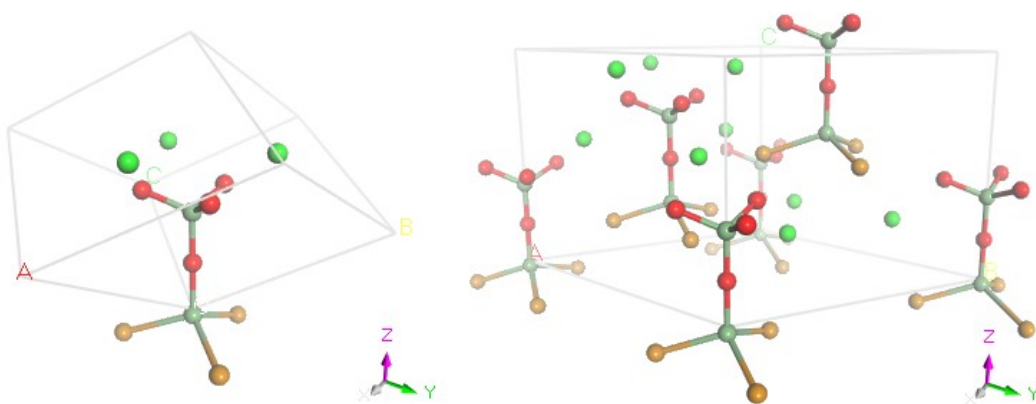
7. Figure S2

Idealized structure merging nearby three 1/3 oxygen ions into a whole one, taking their averaged position, in rhombohedral (left) and hexagonal (right) unit cell.

8. Figure S3

(a)

Electron Image 1

(b)

Element	Atomic%
O K	38.54
Ge K	15.57
Sr L	22.22
Te L	23.67
Totals	100.00

(c)
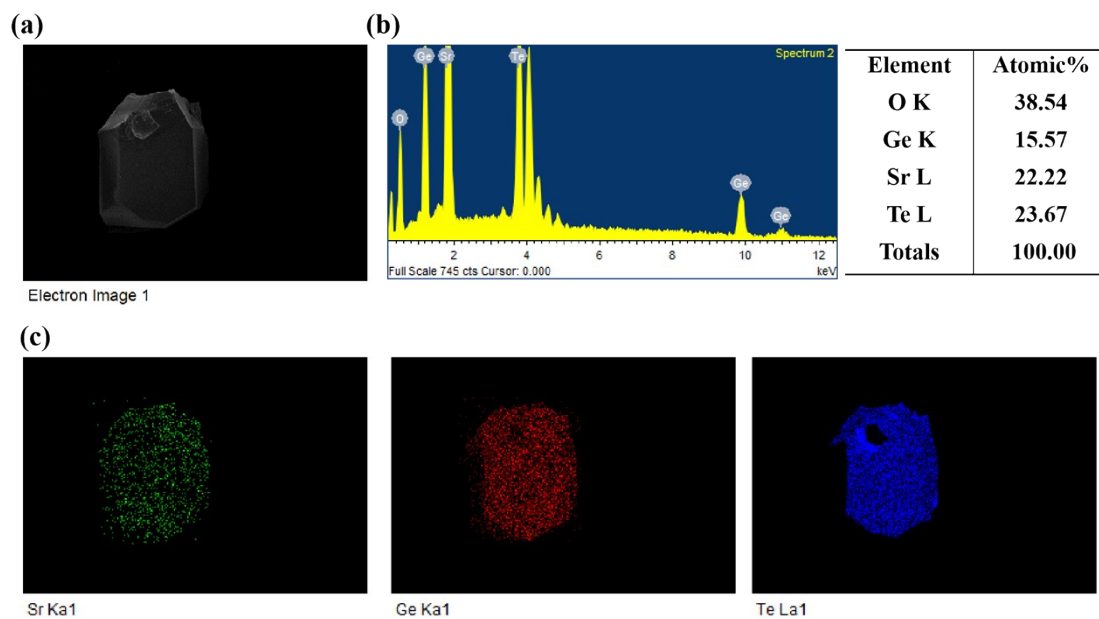
(a) Scanning electron microscopy (SEM) image of $Sr_3Ge_2O_4Te_3$; (b) Elemental analysis of $Sr_3Ge_2O_4Te_3$ by EDX spectroscopy. (c) Elemental distribution of the as-grown crystal.

9. Figure S4
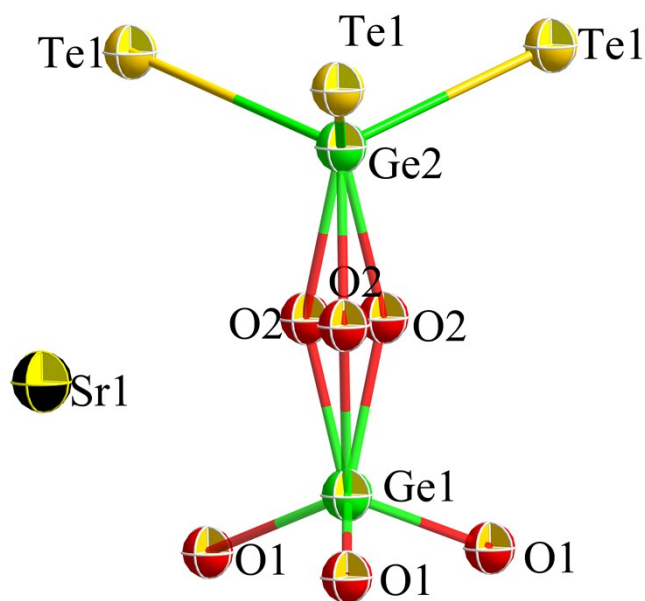
Thermal ellipsoid diagram of $Sr_3Ge_2O_4Te_3$.

10. Figure S5
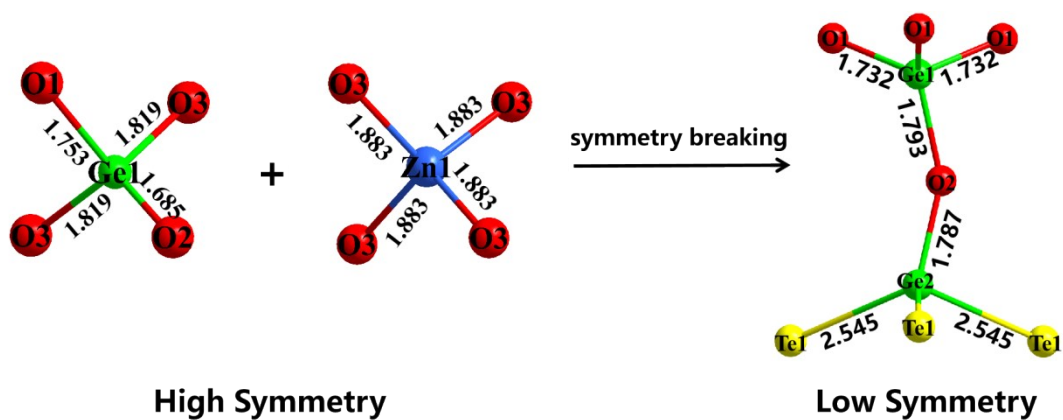
Coordination environment of tetrahedral [GeO$_4$], [ZnO$_4$] , and heteroligand [Ge$_2$O$_4$Te$_3$] ABBs

with the bond distances marked.

11. Figure S6
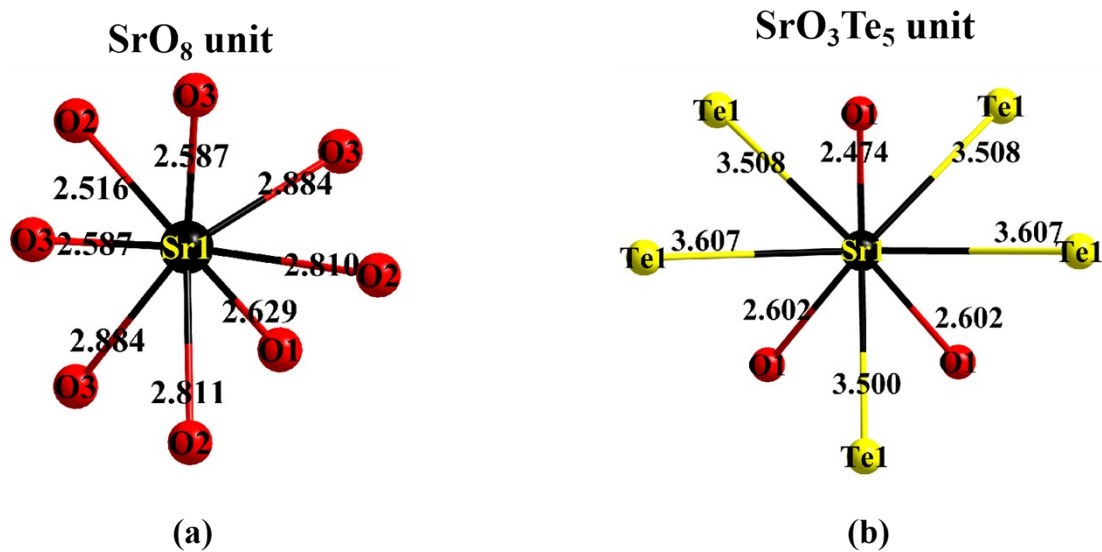
BBBs of [SrO$_8$] (a) and [SrO$_3$Te$_5$] (b) polyhedra in Sr$_2$ZnGe$_2$O$_7$ and Sr$_3$Ge$_2$O$_4$Te$_3$, respectively.

12. Figure S7

(a)

(b)

(a) IR spectrum of $Sr_3Ge_2O_4Te_3$ powder. (b) Raman spectrum of $Sr_3Ge_2O_4Te_3$ powder.
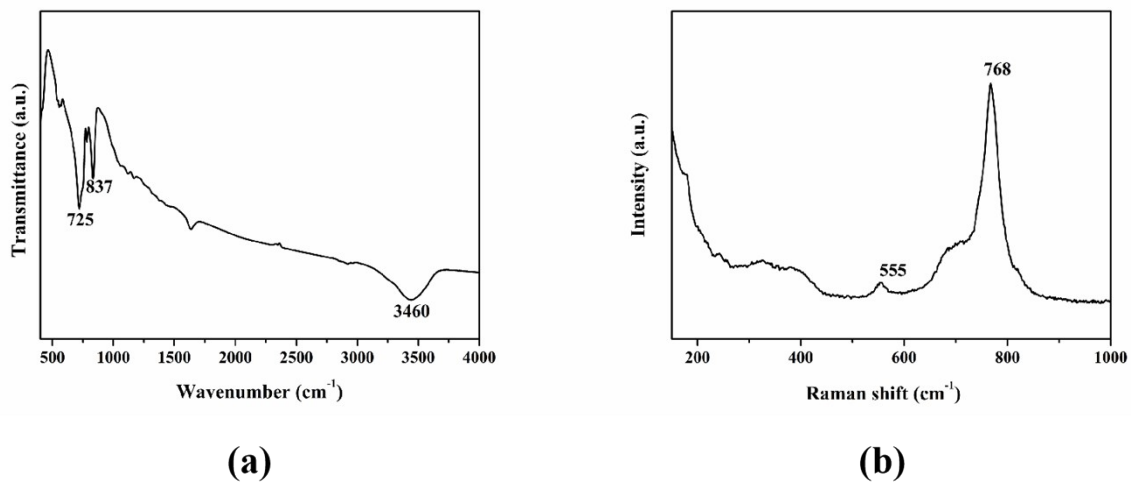
13. Figure S8
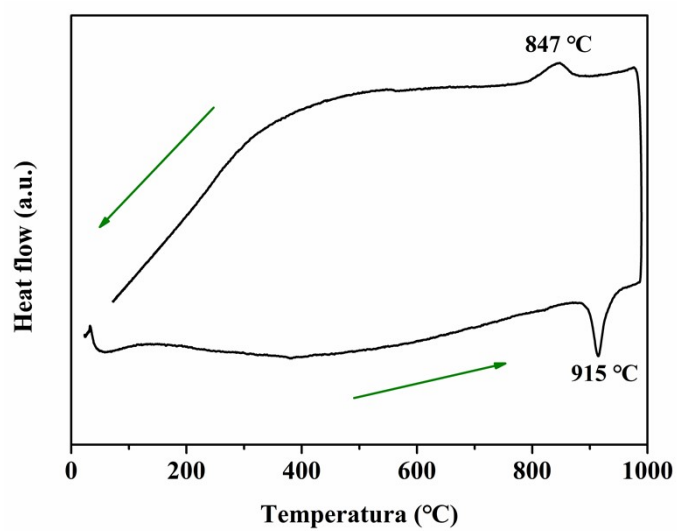
DSC curve of $Sr_3Ge_2O_4Te_3$.

14. Table S1 Crystallographic data and structure refinement for $Sr_3Ge_2O_4Te_3$.

Empirical formula	$Sr_3Ge_2O_4Te_3$
Formula Weight	854.84
Crystal System	trigonal
Space Group	*R3m*
T/K	297(2)
a(Å)	10.5223(18)
b(Å)	10.5223(18)
c(Å)	8.680(2)
α (°)	90
β (°)	90
γ(°)	120
V(Å^3)	832.3(3)
Z	3
ρ_{calc} (g/cm^3)	5.117
M (mm^{-1})	27.385
Radiation	Mo K$_\alpha$ (λ=0.71073)
2θ range for data	6.482 to 66.508
Index ranges	$-15 \leq h \leq 16$, $-14 \leq k \leq 15$, $-6 \leq l \leq 13$
Reflections collected	3004
Independent reflections	[R_{int} = 0.0673, R_{sigma} = 0.0686]
GoF on F^2	1.051
Final R indexes [I>=2σ (I)]	R_1 = 0.0339, wR_2 = 0.0476
Final R indexes [all data]	R_1 = 0.0528, wR_2 = 0.0530

15. Table S2 Atomic coordinates ($\times 10^4$), equivalent isotropic displacement parameters ($\text{Å}^2 \times 10^3$), Wyckoff sites, and bond valence sums (BVS) for $Sr_3Ge_2O_4Te_3$.

Atom	Wyckoff site	x	y	z	U_{eq}	BVS
Sr1	9b	0.85759(7)	0.71518(14)	0.59615(15)	0.0148(4)	1.734
Ge1	3a	0.6667	0.3333	0.7091(3)	0.0085(5)	4.012
Ge2	3a	0.6667	0.3333	0.3096(3)	0.0160(6)	4.027
O1	9b	0.7550(5)	0.5100(10)	0.7828(10)	0.016(2)	−1.967
O2	9b	0.6909(13)	0.3820(30)	0.5090(30)	0.026(9)	−1.785
Te1	9b	0.40312(10)	0.20156(5)	0.21258(10)	0.0170(3)	−1.853

16. Table S3 Selected Bond Lengths (Å) and Angles (°) for $Sr_3Ge_2O_4Te_3$.

Lengths(Å)			
Sr1—O1	2.474(9)	Ge1—O1	1.732(9)
Sr1—O1[7]	2.602(5)	Ge1—O1[2]	1.732(9)
Sr1—O1[8]	2.602(5)	Ge1—O2	1.79(3)
Sr1—O2	3.13(2)	Ge2—O2	1.78(3)
Sr1—Te1[9]	3.5083(14)	Ge2—O2[1]	1.78(3)
Sr1—Te1[10]	3.6069(10)	Ge2—O2[2]	1.78(3)
Sr1—Te1[1]	3.4995(18)	Ge2—Te1	2.5450(13)
Sr1—Te1[11]	3.5083(14)	Ge2—Te1[1]	2.5450(13)
Sr1—Te1[12]	3.6070(10)	Ge2—Te1[2]	2.5450(13)

Angles(°)			
O1[1]– Ge1– O1	107.2(3)	O2[1]– Ge2– O2[2]	24.8(13)
O1[1]– Ge1– O1[2]	107.2(3)	O2[1]– Ge2– O2	24.8(13)
O1– Ge1– O1[2]	107.2(3)	O2[1]– Ge2– O2	24.8(13)
O1[1]– Ge1– O2	118.2(4)	O2[1]– Ge2– Te1[1]	115.9(3)
O1– Ge1– O2	97.4(8)	O2[1]– Ge2– Te1[2]	95.0(8)
O1[1]– Ge1– O2[2]	118.2(4)	O2[2]– Ge2– Te1[2]	115.9(3)
O1– Ge1– O2[2]	118.2(4)	O2– Ge2– Te1[1]	95.0(8)
O1[1]– Ge1– O2[1]	97.4(8)	O2[2]– Ge2– Te1[1]	116.0(3)
O1[2]– Ge1– O2[1]	118.2(4)	O2[2]– Ge2– Te1	95.0(8)
O1[2]– Ge1– O2	118.2(4)	O2[1]– Ge2– Te1[2]	116.0(3)
O1– Ge1– O2[1]	118.2(4)	O2– Ge2– Te1	115.9(3)
O1[2]– Ge1– O2[2]	97.4(8)	Te1[2]– Ge2– Te1	109.62(6)
O2[1]– Ge1– O2[2]	24.7(14)	Te1[2]– Ge2– Te1[1]	109.62(6)
O2– Ge1– O2[2]	24.7(14)	Te1[1]– Ge2– Te1	109.62(6)
O2[1]– Ge1– O2	24.7(14)		

[1]1+Y-X,1-X,+Z; [2]1-Y,+X-Y,+Z; [3]5/3-Y,1/3+X-Y,1/3+Z; [4]2/3+Y-X,4/3-X,1/3+Z; [5]-1/3+X,-2/3+Y,1/3+Z; [6]1/3+X,2/3+Y,-1/3+Z; [7]4/3-Y,2/3+X-Y,-1/3+Z; [8]1/3+X,2/3+Y,2/3+Z; [9]4/3-Y,2/3+X-Y,2/3+Z; [10]2/3+X,1/3+Y,1/3+Z; [11]2/3-Y,1/3+X-Y,1/3+Z; [12]4/3+Y-X,5/3-X,-1/3+Z; [13]2/3+Y-X,4/3-X,-2/3+Z; [14]1/3+Y-X,2/3-X,-1/3+Z; [15]-1/3+X,-2/3+Y,-2/3+Z; [16]-2/3+X,-1/3+Y,-1/3+Z

17. Table S4 Calculated results of fixed cell and ionic geometry

Scissors Correction (eV)	Method	Birefringence	d_{ij} (pm/V)					
0.0	SOS Optics (1064nm)	n_e= 2.30997 n_o= 2.50621 Δn= -0.19624	d_{11}= -1.54 d_{21}= d_{24} d_{31}= d_{15}	d_{12}= 1.54 d_{22}= 0.0 d_{32}= d_{24}	d_{13}= 0.0 d_{23}= 0.0 d_{33}= -2.14	d_{14}= 0.0 d_{24}= 1.70 d_{34}= d_{23}	d_{15}= -1.7 d_{25}= d_{16} d_{35}= d_{13}	d_{16}= 0.0 d_{26}= d_{12} d_{36}= d_{14}
0.0	E-field DFPT	n_e= 2.15702 n_o= 2.29083 Δn= -0.13381	-8.09053 -0.00003 -10.63557	7.65460 -0.00004 -10.41804	-0.19317 -0.19305 -5.42137	-0.31993 -10.41804 -0.19305	-10.63557 -0.31993 -0.19317	-0.00003 7.65460 -0.31993
0.542	SOS Optics (1064nm)	n_e= 2.22207 n_o= 2.38725 Δn= -0.16518	d_{11}= -1.096 d_{21}= d_{24} d_{31}= d_{15}	d_{12}= 1.097 d_{22}= 0.0 d_{32}= d_{24}	d_{13}= 0.0 d_{23}= 0.0 d_{33}= -1.26	d_{14}= 0.0 d_{24}= -0.96 d_{34}= d_{23}	d_{15}= -0.916 d_{25}= d_{16} d_{35}= d_{13}	d_{16}= 0.0 d_{26}= d_{12} d_{36}= d_{14}
0.542	E-field DFPT	n_e= 2.09279 n_o= 2.21279 Δn= -0.12000	-7.20827 -0.00007 -8.78447	6.87490 -0.00000 -8.61817	-0.13645 -0.13633 -4.60955	-0.23458 -8.61817 -0.13633	-8.78447 -0.23458 -0.13645	-0.00007 6.87490 -0.23458

18. Table S5 Calculated results of relaxed cell and ionic geometry

Scissors Correction (eV)	Method	Birefringence	d_{ij} (pm/V)					
0.0	SOS Optics (1064nm)	n_e= 2.32961 n_o= 2.52958 Δn= -0.19997	d_{11}= -1.776 d_{21}= d_{24} d_{31}= d_{15}	d_{12}= 1.776 d_{22}= 0.0 d_{32}= d_{24}	d_{13}= 0.0 d_{23}= 0.0 d_{33}= -2.386	d_{14}= 0.0 d_{24}= -2.022 d_{34}= d_{23}	d_{15}= -2.022 d_{25}= d_{16} d_{35}= d_{13}	d_{16}= 0.0 d_{26}= d_{12} d_{36}= d_{14}
0.0	E-field DFPT	n_e= 2.15702 n_o= 2.29083 Δn= -0.13381	-9.35656 -0.00014 -12.09598	8.84254 -0.00002 -11.83940	-0.18819 -0.18796 -5.72437	-0.32893 -11.83940 -0.18796	-12.09598 -0.32893 -0.18819	-0.00014 8.84254 -0.32893
0.555	SOS Optics (1064nm)	n_e= 2.2355 n_o= 2.4010 Δn= -0.1655	d_{11}= -1.230 d_{21}= d_{24} d_{31}= d_{15}	d_{12}= 1.230 d_{22}= 0.0 d_{32}= d_{24}	d_{13}= 0.0 d_{23}= 0.0 d_{33}= -1.374	d_{14}= 0.0 d_{24}= -1.113 d_{34}= d_{23}	d_{15}= -1.113 d_{25}= d_{16} d_{35}= d_{13}	d_{16}= 0.0 d_{26}= d_{12} d_{36}= d_{14}
0.555	E-field DFPT	n_e= 2.10540 n_o= 2.21613 Δn= -0.11073	-8.26509 -0.00016 -9.93456	7.87786 0.00001 -9.74132	-0.13400 -0.13378 -4.88155	-0.23928 -9.74132 -0.13378	-9.93456 -0.23928 -0.13400	-0.00016 7.87786 -0.23928

References

1. Sheldrick, G., Acta Crystallogr. C **2015,** 71 (1), 3-8.
2. Kurtz, S.; Perry, T., J. Appl. Phys. **1968,** 39 (8), 3798-3813.
3. Clark, S. J.; Segall, M. D.; Pickard, C. J.; Hasnip, P. J.; Probert, M. I.; Refson, K.; Payne, M. C., Z. Krist.-Cryst. Mater. **2005,** 220 (5-6), 567-570.
4. Kohn, W.; Sham, L. J., Phys. Rev. **1965,** 140 (4A), A1133.
5. Hohenberg, P.; Kohn, W., Phys. Rev. **1964,** 136 (3B), B864.
6. Rappe, A. M.; Rabe, K. M.; Kaxiras, E.; Joannopoulos, J. D., Phys. Rev. B **1990,** 41 (2), 1227-1230.
7. Lin, J. S.; Qteish, A.; Payne, M. C.; Heine, V., Phys. Rev. B **1993,** 47 (8), 4174-4180.
8. Lin, J.; Lee, M.-H.; Liu, Z. P.; Chen C. T.; Pickard, C. J., Phys. Rev. B: Condens. Matter Mater. Phys., **1999,** *60*, 13380–13389.
9. Milman, V.; Refson, K.; Clark, S.; Pickard, C.; Yates, J.; Gao, S. P.; Hasnip, P.; Probert, M.; Perlov, A.; Segall, M., J. Mol. Struc.: THEOCHEM **2010,** 954 (1-3), 22-35.
10. Refson, K.; Tulip, P. R.; Clark, S. J., *Phys. Rev. B* **2006,** *73* (15), 155114.
11. Miwa, K., *Phys. Rev. B* **2011,** *84* (9), 094304.